We would like to thank Dr A. Olsen for many stimulating discussions and Professor H. Hashimoto for reviewing the manuscript.

References

FU, P. Q., KONG, Y. H. & ZHANG, L. (1979). *Geochimica*, No. 2, pp. 103–119 (in Chinese).

ISHIZUKA, K. (1982). *Acta Cryst.* A**38**, 773–779.

KITAMURA, M., SHEN, B. M., BANNO, S. & MORIMOTO, N. (1984). *Am. Mineral.* **69**, 154–160.

LI, F. H., LIU, W., KONG, Y. H. & FU, P. Q. (1981). *Kexue Tongbao*, **10**, 590–592 (in Chinese).

SHEN, B. M., TAMADA, O., KITAMURA, M. & MORIMOTO, N. (1982). *Sci. Geol. Sin.* No. 3, pp. 341–342 (in Chinese).

Acta Cryst. (1986). B**42**, 21–25

A New Intermetallic Tetrahedrally Close-Packed Structure with Juxtaposed Pentagonal Antiprisms Determined by High-Resolution Electron Microscopy

BY D. N. WANG, H. Q. YE AND K. H. KUO

Institute of Metal Research, Academia Sinica, 110015 *Shenyang, People's Republic of China*

(*Received* 7 *January* 1985; *accepted* 7 *June* 1985)

Abstract

A new intermetallic tetrahedrally close-packed phase, called the *C* phase, was found coexisting with the *C*14 Laves phase by means of high-resolution electron microscopy and selected-area electron diffraction. Its space group and lattice parameters are: $B2/m$, $a = 17{\cdot}8$, $b = 7{\cdot}7$, $c = 4{\cdot}7$ Å, $\gamma = 99°$ and $Z = 50$ (e.s.d.'s of lattice parameters *ca* 0·05 Å). Its atomic coordinates and orientation relationships with the *C*14 Laves phase have also been determined.

1. Introduction

A number of tetrahedrally close-packed (t.c.p.) phases, such as σ, μ, Laves, *etc.*, are known to exist in many binary and ternary alloys of transition metals as well as in many industrial steels and superalloys. Frank & Kasper (1959) have shown that these t.c.p. structures consist of juxtaposed hexagonal (*e.g.* σ) or pentagonal (*e.g.* μ and Laves phases) antiprisms. In the former case, a number of new phases have recently been found coexisting with the σ phase and their structures have been inferred from high-resolution electron images (Ye & Kuo, 1984; Ye, Li & Kuo, 1984; Li & Kuo, 1986). One of these phases has also been determined by the convergent-beam electron diffraction technique (Lin & Steeds, 1986). Since these phases occurred in intimate intergrowth with σ and also with each other and their dimensions seldom exceeded 1 μm, high-resolution electron microscopy (HREM) and selected-area electron diffraction (SAD) seem to be the only measures one can take to solve their structures.

The t.c.p. structures with juxtaposed pentagonal antiprisms in general (Ye, Li & Kuo, 1985) and the domain structure of the *C*14 Laves phase in particular (Ye, Wang & Kuo, 1985*a*) have recently been discussed. It was shown that when faults occur in $(1\bar{1}\bar{1})$ or $(1\bar{1}0)$ in the *C*14 Laves phase, single slabs of μ structure are generated at the domain boundaries (Fig. 1) and if such faults occur periodically on every other $(1\bar{1}\bar{1})$ or $(1\bar{1}0)$ plane a structure consisting of alternate μ and *C*14 Laves slabs will result. This structure is similar to the *C* silicide $V_2(Co_{0\cdot57}Si_{0\cdot43})_3$ reported earlier (Bardos & Beck, 1966; Kripyakevich & Yarmolyuk, 1971) and it is therefore simply called the *C* phase and occurs generally in intimate intergrowth with the heavily faulted *C*14 Laves phase (Fig. 2). The structure of this *C* phase and its orientation relationships with the *C*14 Laves phase have been studied by means of HREM and SAD and the results are presented in the following.

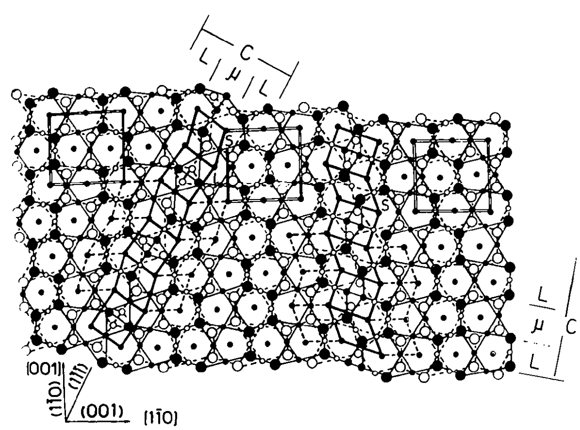

Fig. 1. A schematic diagram illustrating slabs of the *C* phases generated from the $(1\bar{1}\bar{1})$ and $(1\bar{1}0)$ faults in the *C*14 Laves phase projected on the (110) plane.

2. Experimental

The Fe-based superalloy used in the present investigation has the following composition (wt%) determined by chemical methods:

Cr	Ni	W	Mo	Al	Ti	Fe
15·0	34·9	2·12	2·01	2·35	2·35	balance.

After heating to 1413 K for 4 h followed by ageing at 973 K for 200 h, the $C14$ Laves phase was extracted electrolytically from this alloy. The electrolyte consists of $3\% FeSO_4 + 3{\cdot}5\% H_2SO_4 + 2\% NaCl + 5\% NaNO_3 + 86{\cdot}5\% H_2O$, and the electrolysis conditions are: $T = 282$–284 K, current density 3–10 mA cm^{-2}. The crystallites were collected on holey-carbon films supported on copper grids. The high-resolution observation was performed with a JEM 200CX electron microscope equipped with a high-resolution goniometer stage. Composition analysis was carried out in a Philips 400T electron microscope with an EDAX 9100 X-ray energy-dispersive spectrometer and standard thin-film correction software supplied by the maker was used.

Image simulation was carried out using the multislice method with a program written by Ishizuka (1982). The optimum defocus value of −673 Å corresponding to the first broad band in the transfer function for $C_s = 1{\cdot}2$ mm at 200 kV was used. By calculating the variations in the statistically independent fluctuations in accelerating voltage and objective current, the half-width of a Gaussian spread of defocus Δ is 70 Å at the experimental gun bias. The semi-angle of convergence of the incident beam, $\theta_c/\lambda = 0{\cdot}032$ rad Å^{-1}, can be estimated from a focused condenser aperture diffraction pattern. The size limited by the objective aperture, $(\sin\theta)/\lambda = 0{\cdot}35$ Å^{-1}, can be measured from a double-exposed diffraction pattern.

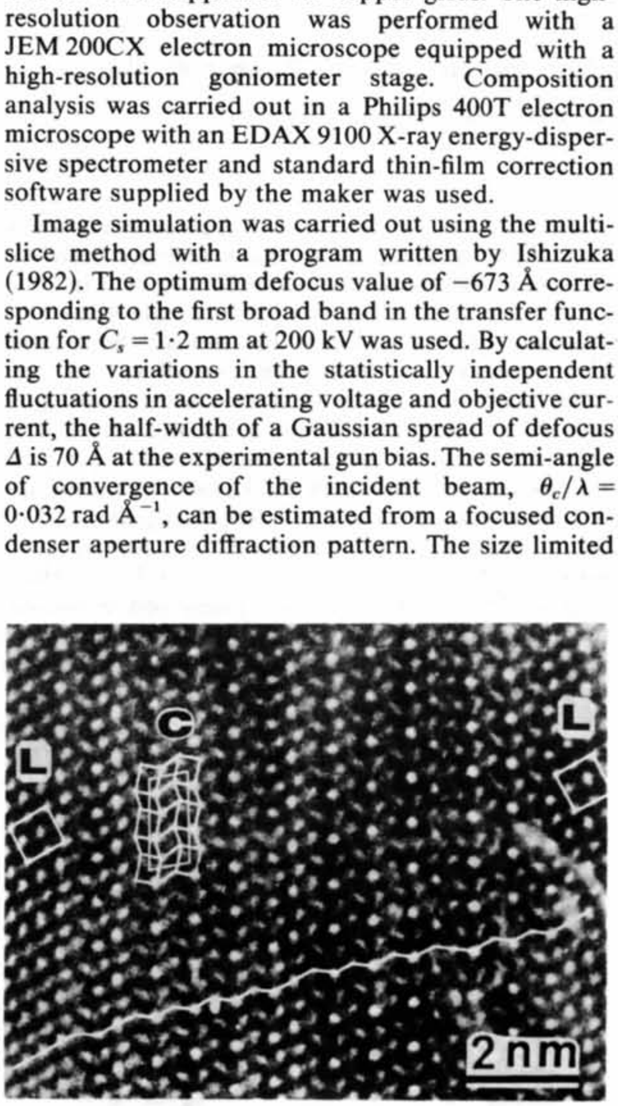

Fig. 2. HREM image of the C phase intimately intergrown with the $C14$ Laves phase where the interphase boundary is $(\bar{1}1\bar{1})_L/(010)_C$. A projected unit cell of C together with the $MgCu_2$ (parallelogram) and Zr_4Al_3 (rectangle) units are outlined. (2 nm ≡ 20 Å.)

3. Structure description

Just as the structure of the H phase has been inferred from that of the σ phase when they occurred side by side in a high-resolution structure image, the structure of the newly found C phase can also be inferred from that of the $C14$ Laves phase when they are imaged together under similar conditions, *i.e.* at a crystal thickness of 50 Å and at optimum defocus as in Fig. 2. Since each bright dot in the image of the $C14$ Laves phase (L in Fig. 2) is known with certainty to represent a pentagonal antiprism, the bright dots in the image of the C phase must also have the same interpretation and a projected unit cell of C together with the $MgCu_2$ (parallellogram) and Zr_4Al_3 (rectangle) units are outlined in Fig. 2. The bright dots represent the positions of the pentagonal antiprisms from which the juxtaposition of these antiprisms in the C phase was derived (Fig. 3). It can be seen that these antiprism columns are arranged in alternating single slabs of μ and $C14$ Laves phases. Evidently, the period in the direction of projection is the height of the double layers of these antiprisms, namely about 4·7 Å. The unit cell of the C phase thus derived from Fig. 2 is monoclinic, as shown in Fig. 3, with $a = 17{\cdot}3$, $b = 7{\cdot}7$, $c = 4{\cdot}7$ Å, $\gamma = 99°$ and $Z = 50$.

From Fig. 3 it is evident that the unit cell is B-centered and there is a mirror plane perpendicular to the twofold rotation axis in the **c** direction. Therefore, the space group is $B2/m$ and the atomic coordinates are given in Table 1. They are exactly the same as those in the $V_2(Co,Si)_3$ phase found earlier by Kripyakevich & Yarmolyuk (1971). However, this new t.c.p. phase is probably an intermetallic phase rather than a silicide since it always occurs in intimate intergrowth with the $C14$ Laves phase. For the same

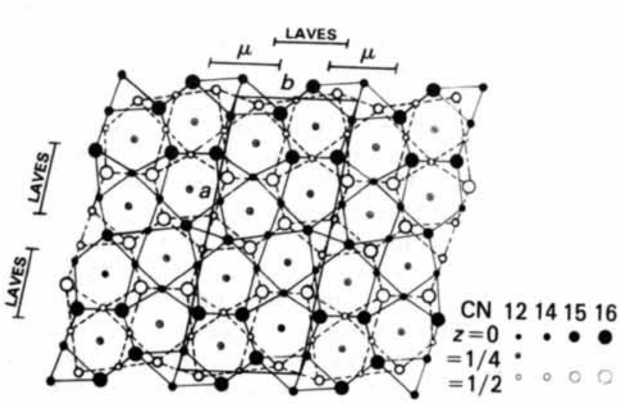

Fig. 3. A (001) projected structure model of the C phase derived from the HREM image with space group $B2/m$ and lattice parameters $a = 17{\cdot}8$, $b = 7{\cdot}7$, $c = 4{\cdot}7$ Å, $\gamma = 99°$.

Table 1. *The atomic coordinates of the C phase*

Number	Position	x	y	z
1	4(i)	0·048	0·367	0·000
2	4(i)	0·208	0·562	0·000
3	4(i)	0·208	0·932	0·000
4	4(i)	0·473	0·817	0·000
5	4(i)	0·069	0·981	0·000
6	4(i)	0·287	0·267	0·000
7	4(i)	0·347	0·543	0·000
8	4(i)	0·375	0·042	0·000
9	4(i)	0·160	0·226	0·250
10	4(i)	0·088	0·695	0·250
11	4(i)	0·160	0·226	0·750
12	4(i)	0·088	0·095	0·750
13	2(c)	0·000	0·500	0·000

reason it is difficult to obtain a separate microanalysis of the *C* phase. We have tentatively assumed that the *C* phase may have a similar composition to that of the *C*14 Laves phase which was determined by X-ray energy-dispersive analysis of several separated Laves particles as $(Fe_{0\cdot16}Cr_{0\cdot10}Ni_{0\cdot06})_2$-$(Mo_{0\cdot14}Ti_{0\cdot10}Al_{0\cdot10}W_{0\cdot02})$. No Si has been detected in the *C*14 Laves phase. However, the possibility of some solute atoms including Si segregating to the *C* phase and making it more stable also exists. A more careful and detailed microanalysis may lead to a better understanding of the formation of the *C* phase.

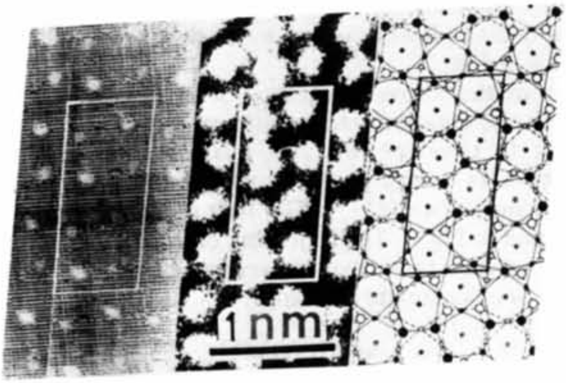

Fig. 4. The [001] structure image (middle) together with the structure model (right) and the simulated image (left) at a thickness of about 50 Å and Scherzer focus.

Fig. 4 shows the [001] structure image (middle) together with the simulated image (left) calculated from the atomic coordinates derived from the structure model (right) by the multislice method. The parameters used for this calculation are: thickness ~50 Å, $\Delta f \sim -500$ to -700 Å, average temperature factor 0·3. The agreement between these two images is fairly good and the one-to-one correspondence between the bright dots in the image and the tunnels inside the pentagonal antiprisms is also obvious. Such a good match may perhaps serve as evidence of the correct interpretation of the observed image and also of the structure derived from it.

The monolinic unit cell of the *C* phase has also been confirmed by the selected-area electron diffraction pattern taken in the [001] direction (Fig. 5) in which a^* and b^* are marked. The calculated dynamical intensities of the *hk*0 reflections are shown on the right of Fig. 5 with filled circles of different sizes according to their intensities and they agree quite well with the observed results. The *hk*0 reflections with *h* odd are missing on account of the *B* centering. Moreover, the outermost ten strong diffraction spots show fivefold symmetry reflecting the presence of pentagonal antiprisms in the *C* phase. This is also a common feature of diffraction patterns of the t.c.p. phases with juxtaposed pentagonal antiprisms (Ye, Wang & Kuo, 1985*b*). All these findings reconfirm the proposed structure model of the *C* phase.

4. Intergrowth structures

One of the most prominent features of the newly found *C* phase is the fact that it generally occurs in intimate intergrowth with the *C*14 Laves phase. This has already been shown in Fig. 2 where the interphase boundary is $(\bar{1}1\bar{1})_L/(010)_C$. Fig. 6 presents another type of intergrowth where the interphase boundary is $(1\bar{1}0)_L/(100)_C$. In both cases there are also domain

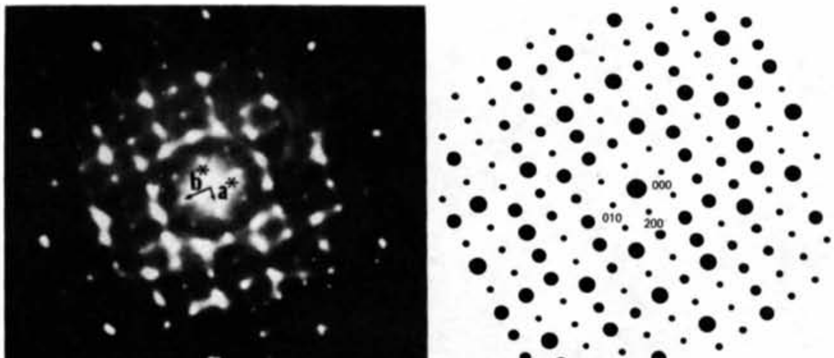

Fig. 5. The [001] electron diffraction pattern of the *C* phase (left) together with that calculated (right) by the multislice method at a crystal thickness of 70 Å. The outermost ten strong spots show fivefold symmetry.

boundaries within each of these two phases so that the structure images resemble mosaic patterns of microdomains. The domain structure in the *C*14 Laves phase has already been discussed (Ye, Wang & Kuo, 1985*a*).

In general, the interphase boundary is not only planar but also in good register with the structures on both sides of it, as can be seen on these two structure images as well as in the schematic drawing in Fig. 1. In other words, one structure converts or passes coherently into the other. This is because these two structures not only consist of the same pentagonal antiprisms but also have similar arrangements of these antiprisms. This is obvious when one considers the structure of the *C* phase as consisting alternately of single slabs of the μ and *C*14 Laves phases. Moreover, the structures of the μ and *C*14 Laves phases also have some common or closely related features.

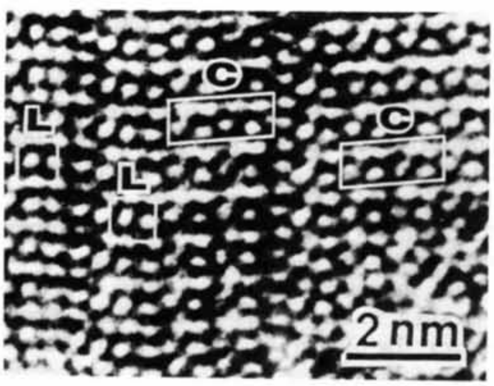

Fig. 6. HREM image of the *C* phase intimately intergrown with the *C*14 Laves phase with interphase boundary $(1\bar{1}0)_L/(100)_C$.

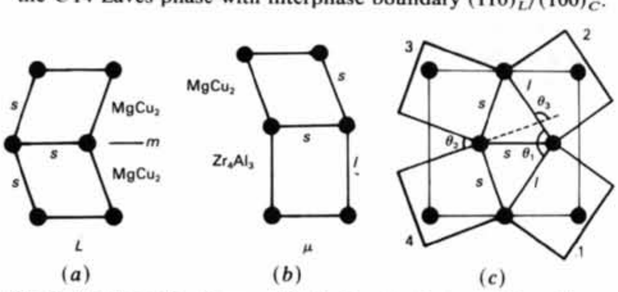

Fig. 7. A schematic diagram illustrating the juxtaposition of pentagonal antiprisms in (*a*) the *C*14 Laves and (*b*) the μ phase and also (*c*) the coexistence of four possible variants of the *C* phase on the same *C*14 Laves matrix.

The filled circles in Fig. 7 represent either the atoms of the second layers at $z=\pm\frac{1}{4}$ or the centers of the pentagonal antiprisms in the μ and *C*14 Laves phases. The juxtaposition of pentagonal antiprisms in the *C*14 Laves phase in turn can be visualized as consisting of two $MgCu_2$ units in mirror reflection and that in the μ phase as a $MgCu_2$ unit joined to a Zr_4Al_3 one. If one calls the $MgCu_2$ and Zr_4Al_3 first-order t.c.p. structures, then the μ and *C*14 Laves may be called second-order, and the *C* phase third-order (Ye, Li & Kuo, 1985). It is of interest to note that the short (s) and long (l) sides of the Zr_4Al_3 rectangle are very close to the lengths of the sides (s) and long diagonal (l) of the $MgCu_2$ parallelogram. Therefore, there are no less than four possible ways to attach a Zr_4Al_3 unit to the *C*14 Laves unit cell. In other words, four variants of non-basal intergrowth structures between the μ and *C*14 Laves phases or rather between the *C* and *C*14 phases can exist and they are numbered 1 to 4 in Fig. 7.

From the above discussion it is obvious that a definite orientation relationship exists between the *C* and *C*14 Laves phases. Fig. 1 is a [110] projection of the *C*14 Laves phase in which a slab of the *C* phase occurs on $(1\bar{1}\bar{1})_L$. The unit cell in this case is outlined in Fig. 3. The following orientation relationship between these two phases can be derived from these two schematic drawings:

$$\begin{aligned}&(010)_C\|(1\bar{1}\bar{1})_L\\&[100]_C\|[1\bar{1}2]_L\qquad\text{variant (1).}\\&[001]_C\|[110]_L\end{aligned}$$

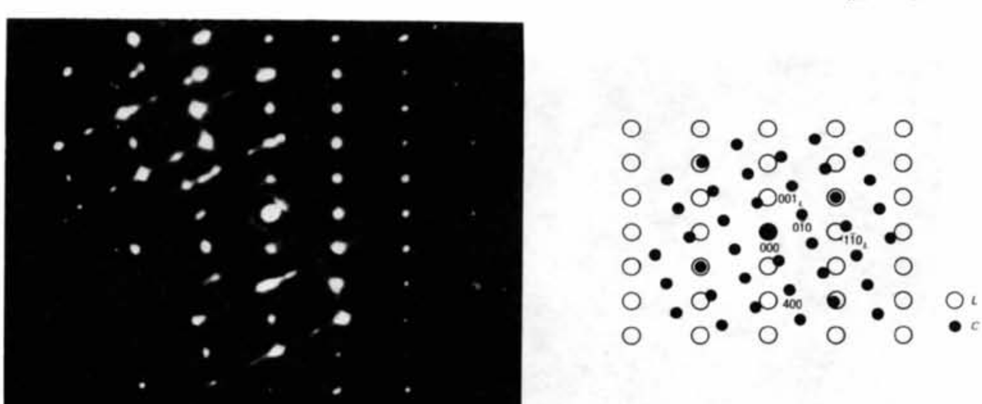

Fig. 8. A composite electron diffraction pattern of the $[001]_C$ and $[110]_L$ patterns showing the orientation relationship $(010)_C\|(1\bar{1}\bar{1})_L$, $[100]_C\|[1\bar{1}2]_L$ and $[001]_C\|[110]_L$.

The unit cells of these two phases are outlined in their structure images respectively in Fig. 2 to show this orientation relationship. However, in this case the interphase boundary is not $(1\bar{1}\bar{1})_L$ but its equivalent $(\bar{1}1\bar{1})_L$ of variant (2). This orientation relationship has also been confirmed by a composite electron diffraction pattern of two phases, *i.e.* a $[001]_C$ pattern superposed on the $[110]_L$ pattern (Fig. 8).

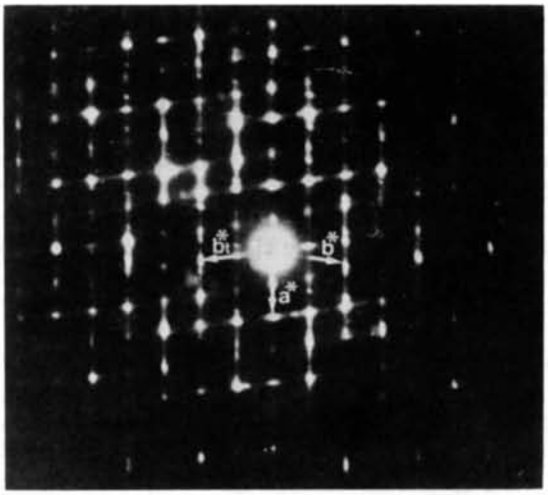

Fig. 9. A composite electron diffraction pattern of variants (3) and (4) of the C phase.

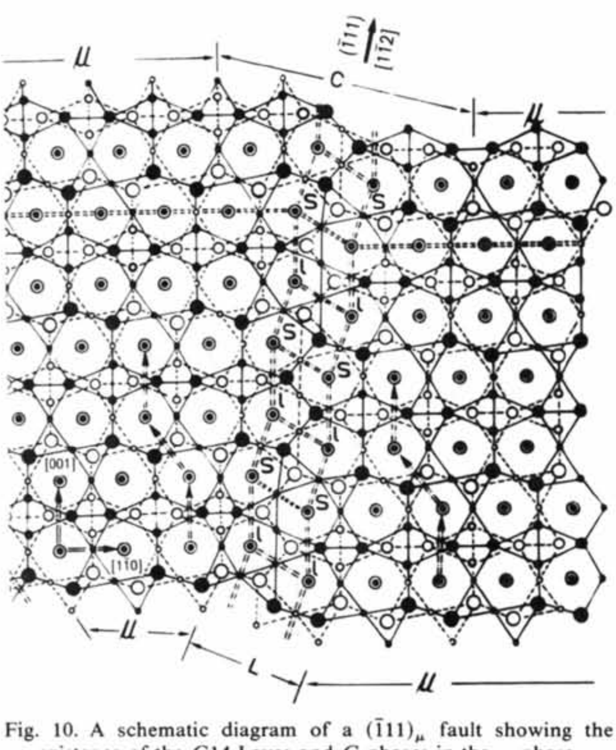

Fig. 10. A schematic diagram of a $(\bar{1}11)_\mu$ fault showing the existence of the C14 Laves and C phases in the μ phase.

This C phase can also appear on $(1\bar{1}0)_L$ as already shown in Figs. 1 and 6, and in this case the interphase boundary is $(100)_C$. Consequently, one can easily obtain a second type of orientation relationship between these two t.c.p. phases:

$$\left.\begin{array}{l}(100)_C \| (1\bar{1}0)_L \\ [010]_C \| [001]_L \\ [001]_C \| [110]_L\end{array}\right\} \text{variant (3).}$$

Fig. 6 shows the structure image of these two phases with such an interphase, though in this case it is variant (4), a mirror reflection of variant (3).

Obviously, there are four possible first-order rotation domains of the C phase with rotation angles $\theta_1 = 110$, $\theta_2 = 40$ and $\theta_3 = 109°$, see Fig. 7. Since in each C domain there are also two differently oriented C14 Laves slabs (see Fig. 3) so that many second-order, and even higher-order, rotation domains may occur. The 109° rotation domains have frequently been observed as can be expected from the structural considerations given in connection with Figs. 1 and 3. Fig. 9 is the composite electron diffraction pattern of variants (3) and (4) which are chemical twins with a glide symmetry relationship.

Since the structure of the t.c.p. phase C can be visualized as consisting alternately of single slabs of the μ and C14 Laves phases, it is naturally expected that the C phase should also be found in intimate intergrowth with the μ phase. Fig. 10 is a schematic drawing of a $(\bar{1}11)_\mu$ fault in the μ phase where a slab of the C14 Laves structure occurred. Such a fault has already been observed (Li & Kuo, 1985). Together with the μ slabs on its two sides, this Laves slab will form a nucleus of the C phase. Or, in other words, if the planar faults occur periodically on every second $(\bar{1}11)_\mu$ plane a single domain of the C phase will be formed in the μ phase.

References

BARDOS, D. I. & BECK, P. A. (1966). *Trans. Am. Inst. Min. Metall. Pet. Eng.* **236**, 64–69.
FRANK, F. C. & KASPER, J. S. (1959). *Acta Cryst.* **12**, 483–499.
ISHIZUKA, K. (1982). *Acta Cryst.* **A38**, 773–779.
KRIPYAKEVICH, P. I. & YARMOLYUK, Y. P. (1971). *Dopov. Akad. Nauk. Ukr. RSR Ser. A*, **32**, 948–951.
LI, D. X. & KUO, K. H. (1985). *Philos. Mag.* **A51**, 849–856.
LI, D. X. & KUO, K. H. (1986). *Acta Cryst.* In the press.
LIN, Y. P. & STEEDS, J. W. (1986). *Acta Cryst.* In the press.
YE, H. Q. & KUO, K. H. (1984). *Philos. Mag.* **A50**, 117–132.
YE, H. Q., LI, D. X. & KUO, K. H. (1984). *Acta Cryst.* **B40**, 461–465.
YE, H. Q., LI, D. X. & KUO, K. H. (1985). *Philos. Mag.* **A51**, 829–837.
YE, H. Q., WANG, D. N. & KUO, K. H. (1985*a*). *Philos. Mag.* **A51**, 839–848.
YE, H. Q., WANG, D. N. & KUO, K. H. (1985*b*). *Ultramicroscopy*, **16**, 273–278.